ELSEVIER

Nuclear Instruments and Methods in Physics Research B 192 (2002) 3–16

NIM B
Beam Interactions with Materials & Atoms

www.elsevier.com/locate/nimb

Low energy positron scattering and annihilation studies using a high resolution trap-based beam

J.P. Sullivan, S.J. Gilbert, J.P. Marler, L.D. Barnes, S.J. Buckman [1], C.M. Surko *

Department of Physics, University of California, San Diego, 9500 Gilman Drive, La Jolla, CA 92093-0319, USA

Abstract

A high resolution positron beam, generated from a Penning–Malmberg trap, has been used for a range of low energy scattering and annihilation studies on atoms and molecules. We describe measurements of total scattering, differential elastic scattering and integral vibrational and electronic excitation cross sections for a number of atoms and molecules using this beam, and compare the absolute cross sections that are obtained with data from electron impact. The first study of annihilation on atoms and molecules as a function of positron energy is described. The results in molecules indicate large resonant enhancements of the annihilation rates at energies corresponding to those of the molecular vibrations. © 2002 Elsevier Science B.V. All rights reserved.

Keywords: Positron; Scattering; Atoms; Molecules; Cross-sections; Annihilation

1. Introduction

The recent realization of a high resolution (~25 meV FWHM) positron beam from a Penning trap [1] has provided an important impetus to study low-energy positron interactions with atoms and molecules. Until this development, the energy resolution that was obtainable with typical positron sources was ~0.5 eV (or worse). In the case of scattering experiments, this severely limited measurements of elastic and total cross sections at energies less than a few electron volts. In the case of positron annihilation, the relatively weak and poor resolution positron sources that were available have precluded, for example studies of annihilation rates as a function of positron energy.

The lack of high resolution positron beams also precluded the investigation of most discrete excitation processes, such as vibrational excitation or electronic excitation, at near-threshold energies. Previous measurements of differential elastic scattering (e.g. Ref. [2]) have provided an interesting test for scattering calculations, but they generally have had a lower energy limit of around 5 eV and have yielded relative cross sections, thus only providing a test of the scattering dynamics via comparison of the *shape* of the differential cross section (DCS). State-resolved measurements of atomic and molecular excitation are equally rare. They have typically been carried out using time-of-flight techniques where the inelastically scattered positrons are temporally separated from the elastic and unscattered beam. Unfortunately,

* Corresponding author. Tel.: +1-858-534-6880; fax: +1-858-534-0173.
E-mail address: csurko@ucsd.edu (C.M. Surko).
[1] Permanent address: Research School of Physical Sciences and Engineering, Australian National University, Canberra.

0168-583X/02/$ - see front matter © 2002 Elsevier Science B.V. All rights reserved.
PII: S0168-583X(02)00700-0

timing resolution constraints have generally resulted in such experiments yielding cross sections for a number, or all, of the vibrationally or electronically excited states in the target.

Not surprisingly perhaps, the small amount of experimental data in these areas has resulted in a similarly small amount of theoretical interest, despite the significant and interesting challenges that such calculations could offer. There have been a number of investigations of vibrational excitation of diatomic molecules (e.g. [3–5]) and polyatomic molecules [6] using approaches such as vibrational close coupling and continuum multiple scattering techniques. Electronic excitation of both atoms and molecules has been studied using distorted-wave [7], close coupling [8] and Schwinger variational [9] techniques.

In another important area of low-energy positron physics, there have been longstanding questions associated with the annihilation of positrons interacting with atoms and molecules at energies below the threshold for positronium formation. Prediction of these annihilation rates requires precise knowledge of electron–positron correlations, and this has proven difficult to calculate with precision even for relatively simple targets. Perhaps *the* key problem in this area, first pointed out by Paul and Saint-Pierre [10] is that positron annihilation rates in many molecular gases are orders of magnitude larger than those expected on the basis of simple collisions [11–15]. There have been a number of proposals to explain these large annihilation rates in terms of some kind of electronic or vibrational resonance or positron–molecule bound state [12,16–19], however microscopic tests of these ideas has proven difficult. In particular, progress has been hindered greatly by the fact that even the enhanced annihilation cross sections observed in hydrocarbons, e.g. are too small to study with conventional positron sources.

In this paper we describe the results of new positron scattering and annihilation experiments. We briefly describe an experimental apparatus for the generation of a high-resolution, trap-based positron beam. When combined with a new technique for scattering in a magnetic field, this has enabled us to measure, in many cases for the first time, a range of low energy scattering phenomena. We illustrate the power of the technique with examples of low energy, absolute elastic DCS, absolute integral cross sections for near-threshold vibrational and electronic excitation and high-resolution measurements of total scattering cross sections in a search for positron–atom (molecule) resonances.

We have also been able to use the cold positron beam to make the first positron annihilation studies of atoms and molecules that are resolved as a function of positron energy. While these experiments are just beginning, the results to date indicate that the large observed enhancements in molecular annihilation rates are closely associated with the excitation of vibrational modes of the positron–molecule complexes. The results are interpreted as the most direct evidence to date that positrons can bind to molecules. A number of important questions can now be addressed using this technique, such as this important issue of positron binding to molecules and tests of predictions for greatly enhanced values of annihilation rates as the positron energy approaches the positronium formation threshold or other inelastic thresholds from below.

2. Positron scattering from atoms and molecules

2.1. Experimental apparatus and scattering technique

The apparatus and experimental techniques used for these studies have been described in detail elsewhere [1,20]. A schematic diagram of the apparatus is shown in Fig. 1. Briefly, a buffer-gas positron accumulator is used to trap and cool positrons emitted from a solid-neon-moderated ^{22}Na source. Collisions with N_2 and CF_4 molecules provide energy loss mechanisms (electronic and rovibrational excitation) for the positron trapping and cooling. Once trapped, the positrons are confined using an electrostatic potential well in the presence of a magnetic field of $\sim$0.1 T. By carefully manipulating the depth of the well, a pulsed beam of positrons can be released from the trap with both a well defined energy and an energy spread as small as 18 meV. In practice, for the experiments

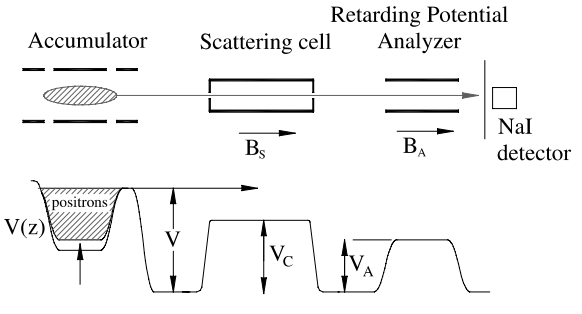

Fig. 1. Schematic diagram of the positron accumulator and scattering apparatus (above) and the associated potential profile (below).

described here, space charge considerations limit the pulses to about 3×10^4 positrons each. The pulse width is $\sim$2 μs, and the repetition rate is typically 4 Hz. The pulsed positron beam is then passed through a scattering cell containing the gas under study. The gas pressure in the scattering cell is typically in the range 0.1–0.5 mTorr while the pressure elsewhere in the system is maintained a factor of $\sim$500 lower by differential pumping. After passing through the collision cell, the positrons are guided through a retarding potential analyzer (RPA). Detection is achieved by measuring the 511 keV annihilation gamma rays which are emitted when the positrons strike a metal collector plate at the end of the RPA. Both the scattering cell and the RPA are located in a magnetic field of variable strength up to $\sim$0.1 T.

In order to measure scattering cross sections in the presence of the magnetic field, we exploit the properties of the positron motion in the field. The total energy of a positron, E_T, can be separated into two components

$$E_T = E_\parallel + E_\perp, \tag{1}$$

where $E_\parallel$ is the energy in the motion parallel to the field and $E_\perp$ is the energy in the cyclotron motion perpendicular to the field. In the present experiments, an incident beam with $E_\parallel \geqslant 0.5$ eV and $E_\perp \approx 0.025$ eV is used. The RPA only measures $E_\parallel$ and any scattering process can redistribute or transfer energy between $E_\parallel$ and $E_\perp$. At the energies considered here, both elastic and inelastic scattering (i.e. rovibrational and electronic excitation) are possible. For each of these processes, the positron can also be scattered through some scattering angle θ. Denoting the initial positron energy as E_i and the total energy of the positron after scattering as E_s then

$$E_s = E_i \quad \text{(elastic scattering)}, \tag{2}$$

and

$$E_s = E_i - E_{ex} \quad \text{(inelastic scattering)}, \tag{3}$$

where E_{ex} is the energy loss involved in an excitation process. For both elastic and inelastic scattering,

$$E_\parallel = E_s \cos^2(\theta), \tag{4}$$

and

$$E_\perp = E_s \sin^2(\theta). \tag{5}$$

Thus the scattered beam will have a distribution of $E_\parallel$ values, and this will be reflected in the signal measured by the RPA.

This is illustrated in the panels of Fig. 2, which shows typical RPA cut-off curves obtained with and without gas in the scattering cell. Without gas in the cell (Fig. 2(a)), positrons are transmitted right up to the cut-off point, and the width of the cut-off is a measure of the energy resolution of the beam. For the measurements discussed here the energy resolution was $\sim$25 meV. With gas in the cell, the effects of scattering can be clearly seen at voltages below the cut-off point in Fig. 2(b). In this region, positrons have lost $E_\parallel$ due to angular scattering in both elastic and inelastic collisions, and they are cut-off at lower RPA voltages. From Eqs. (1)–(5), it can be seen that this collisional loss of $E_\parallel$ will extend all the way back to zero energy. For example, in an elastic collision at $\theta = 90°$, $E_\parallel = 0$ and $E_\perp = E_s$. We note that, if $\theta > 90°$, the positrons are scattered back toward the trap, but they are then reflected from the potential wall that defines the end of the trap and pass through the gas cell again. Thus it is impossible to distinguish between scattering through $\theta°$ and $(180 - \theta)°$. If the scattering is purely elastic the scattering angle can be obtained from

$$\theta = \cos^{-1}\sqrt{E_\parallel / E_s}, \tag{6}$$

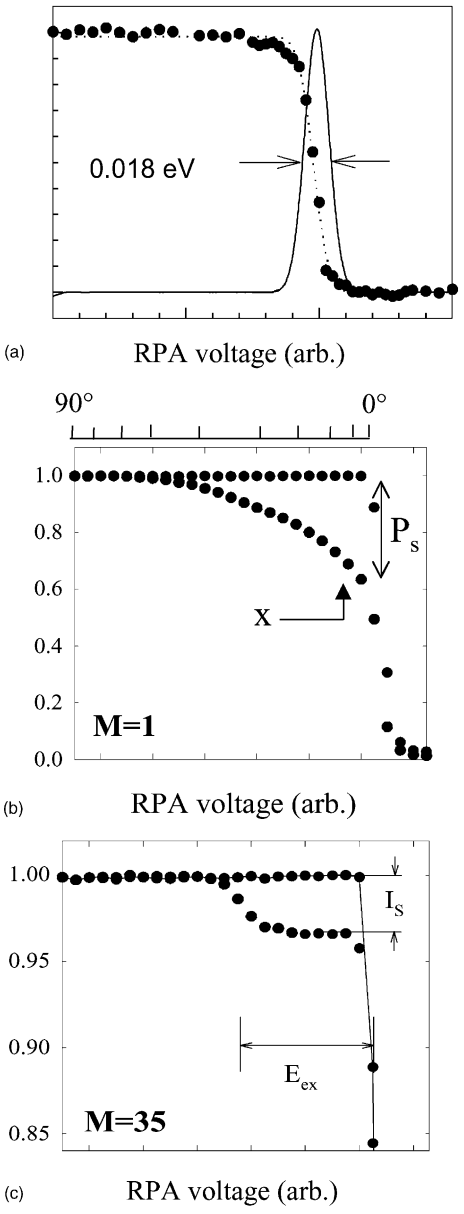

Fig. 2. RPA cut-off curves. (a) No gas in scattering cell. (b) Test gas (in this case CO) in the cell and with a ratio of B fields between the gas cell and RPA, $M = B_s/B_a = 1$. The point 'X' is the voltage at which the total cross section measurements are performed, and P_s represents the probability of scattering. (c) Test gas in the scattering cell and $M = 35$. Note the step in the RPA curve at the excitation energy for the $v = 1$ mode in CO.

and the *differential scattering cross section* is given by

$$\frac{d\sigma}{d\Omega} = C\sqrt{E_s E_\parallel}\left(\frac{dI(E_\parallel)}{dE_\parallel}\right), \tag{7}$$

where $I(E_\parallel)$ is the normalized signal measured with the RPA, and the constant C depends on the gas number density and cell length.

The RPA curve represents an integral spectrum. Thus, if the transmitted positron signal at a voltage close to the beam energy cut-off is monitored (e.g. at the point labeled by 'X' in Fig. 2(b)), then the difference between this signal level and the unscattered beam (normalized to unity), is the probability of any scattering event having occurred. This is denoted by P_s in Fig. 2(b) and it is related to the *total scattering cross* section (Q_t) by

$$Q_t = \frac{P_s}{nl}, \tag{8}$$

where n is the gas number density and l the distance over which the scattering takes place [20]. In the present experiments, l is taken to be the physical length of the scattering cell (38.1 cm). To ensure that the spread in beam energy does not effect the measurement, the voltage at point 'X' is chosen to be three standard deviations (~40 meV) from the beam cut-off. By measuring the signal at point 'X' as a function of energy, the energy dependence of the total scattering cross section can be obtained.

In order to discriminate between those scattering processes that change $E_\parallel$ as a result of angular scattering and those involving a discrete energy loss, we take advantage of a property of the motion of positrons in a slowly varying magnetic field, namely that the quantity $E_\perp/B$ is an invariant. If we analyze the transmitted positrons in a magnetic field which is much smaller than that in which they are scattered, then most of $E_\perp$ is converted to $E_\parallel$. In this case energy loss processes can be distinguished by the distinct "steps" that they produce in the RPA curve. Such a measurement is shown in Fig. 2(c) for vibrational excitation in CO. Here the ratio of the magnetic field, B_s, in the scattering cell to the magnetic field, B_a, in the analyser is $M = B_s/B_a = 35$. Once again, the height of the step in the cut-off curve is directly proportional to the *integral cross section* for the inelastic scattering process.

Thus, by an appropriate choice of scattering and analysis conditions, a range of absolute scattering cross sections can be measured with this relatively simple technique. In these experiments, the absolute energy scale is established by calibrating the potential difference between the positron source and the scattering cell against the known threshold energy for a process such as vibrational excitation. The estimated uncertainty in the beam energy is ~25 meV. At these levels of precision, it is important to ensure the uniformity of the potential in the scattering cell. This is measured using the cold positron beam, by measuring the time delay of the beam as it passes through the scattering cell as a function of the energy of the positron beam. Potential uniformities as low as a few meV (rms) have been achieved. Typical values are ~25 meV (rms).

3. Scattering results

3.1. Elastic scattering

Examples of recent measurements of elastic DCS are shown in Fig. 3(a) and (b). In Fig. 3(a) we show the absolute elastic DCS for scattering from H_2 at an energy of 0.5 eV, which is just below the threshold for excitation of the first vibrational mode of this molecule. Thus, this measurement is vibrationally elastic but constitutes a sum over open rotational excitation channels. While the reduced angular range is a drawback of the technique, particularly at low energies, this is the first absolute elastic DCS measurement for positron scattering from a molecule, and it provides an important opportunity for comparison with theory for the simplest positron–molecule scattering system. In Fig. 3(a) we show results from a Kohn variational calculation [21], and the distributed positron model (DPM) calculation [22]. In order to make a more realistic comparison with the experiment, which simultaneously measures contributions at $\theta°$ and $(180-\theta)°$, we have summed the forward and backward contributions in the theory. While the DPM calculation provides the best agreement with the experiment, there remain clear differences between experiment and theory, even for this the simplest diatomic molecule.

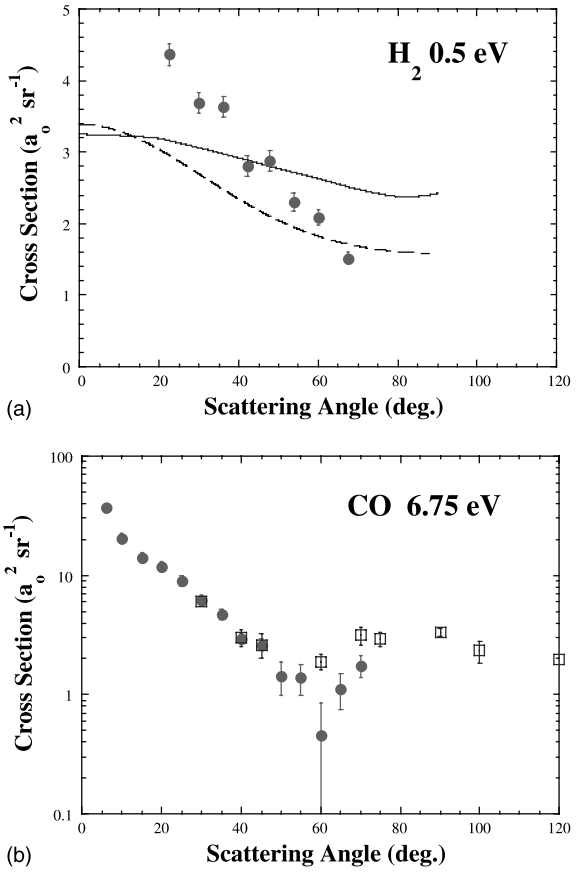

Fig. 3. (a) Elastic differential scattering cross sections for H_2 at 0.5 eV. (•) present experimental data, (—) a Kohn variational calculation [21] and (– – –) a calculation using the DPM [22]. (b) Elastic differential scattering cross sections for CO at 6.75 eV. (•) present measurements, (□) measurements of the Detroit group [24], which were normalised to the present data at 45°.

In Fig. 3(b) we show data for the absolute DCS for scattering from CO at an energy of 6.75 eV. This cross section is "quasi-elastic" in the sense that it includes contributions from open inelastic channels (vibration and rotation). However, as these are known to contribute less than about 5% of the total scattering cross section at this energy [23], this measurement is essentially the elastic DCS. This particular measurement was motivated by a recent, relative DCS measurement at this energy by the Detroit group [24] who were investigating diffraction minima in the cross sections for

various diatomic molecules. Their data are also shown on this plot, normalized to the present results at an angle of 45°. The agreement is very good. Note also the unusually large value of the forward scattering cross section for this mildly polar molecule. Unfortunately, for this molecule there are presently no theoretical calculations with which to compare.

3.2. Vibrational excitation

The combined techniques of the trap-based, high-resolution positron beam and scattering in a magnetic field have been used recently to measure the first absolute integral cross section (ICS) for vibrational excitation of a range of molecules [23,25]. For these measurements, the RPA curves are obtained with a lower magnetic field in the analyser region and they have an appearance similar to that shown in Fig. 2(c). We show examples of these cross sections for H_2 and CH_4 in Figs. 4 and 5.

For molecular hydrogen, the data show a relatively small peak in the ICS near threshold, with a magnitude of about 0.4 a_0^2. The cross section drops quickly at higher energies. There are three calculations with which to compare the experimental data. There is reasonable agreement with the most recent of these calculations [3,26], while the data

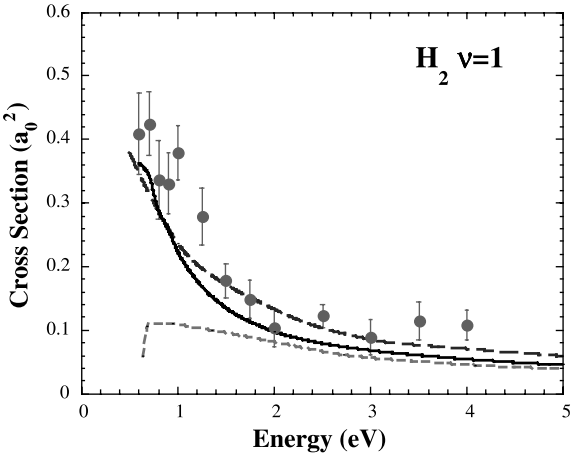

Fig. 4. Absolute integral cross sections for the excitation of the $v = 1$ vibrational mode of H_2. (•) present data, (– – –) calculation of [3], (- - -) calculation of [27], (—) calculation of [26].

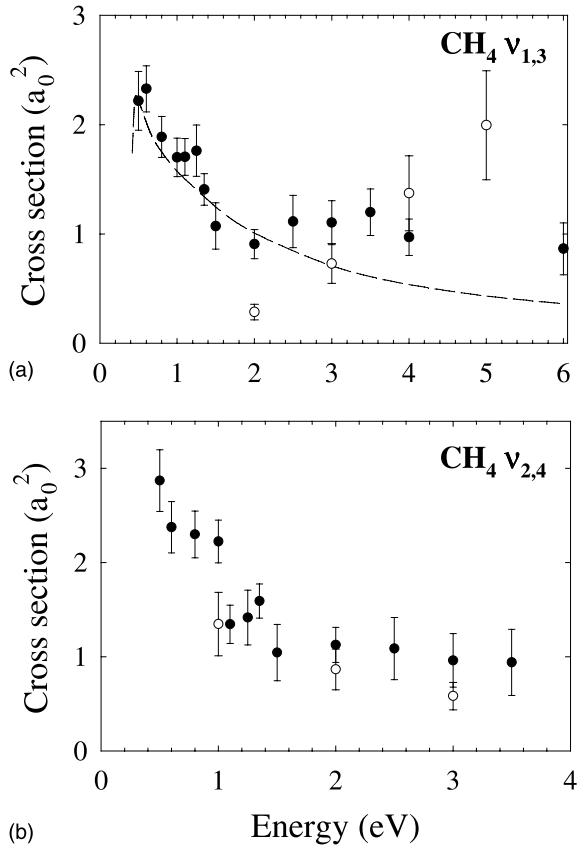

Fig. 5. Absolute integral cross sections for the excitation of the (a) $\nu_{1,3}$ and (b) $\nu_{2,4}$ hybrid modes of CH_4. (•) present positron data, (– – –) calculation of [28]; and (○) the electron scattering data of [43].

are substantially larger than the earliest calculation [27]. Note that the recent calculation of Gianturco and Mukherjee [26] corrects an earlier version [5] which was substantially lower in magnitude than the present data.

For methane, there are four low-lying vibrational modes. Two of these are infra-red active, the ν_3 and ν_4 modes at 0.374 and 0.162 eV. They are nearly degenerate with the ν_1 and ν_2 Raman-active modes at 0.362 and 0.190 eV. The excitation cross sections for these hybrid pairs $\nu_{2,4}$ (bending) and $\nu_{1,3}$ (stretching), which are not resolvable with the present energy resolution, are shown in Fig. 5(a) and (b) respectively. The $\nu_{1,3}$ cross section is compared with a recent 3-state close-coupling calculation [28]. The agreement is very encouraging.

For the $v_{2,4}$ mode there are presently no theoretical calculations available for comparison.

3.3. Electronic excitation

Recently, the first state-resolved measurements of electronic excitation by positron impact have also been made (i.e. for Ar, H_2 and N_2) using the trap-based beam [29]. In these studies, the RPA curves (which provide integral energy-loss spectra) are considerably simplified as compared with those measured for electrons, due to the lack of the excitation of triplet states via the exchange interaction in the positron case. These simplified spectra have allowed us to isolate individual vibrational levels within the electronic excitation manifolds. An example of such a spectrum for N_2 is shown in Fig. 6 at an incident energy of 11 eV. At this energy, three electronically excited channels are open, the $a'^1\Sigma$, $a^1\Pi$ and $w^1\Delta$ states. By fitting these spectra with a series of overlapping error functions weighted by the known Franck–Condon factors for the vibrational levels, and considering the individual excitation cross sections as free parameters, the integral scattering cross sections for each of these states can be obtained. In Fig. 6 the solid line is an example of such a fit. For the energies considered here, it was found that the $w^1\Delta$ state plays little role in the excitation process at near-threshold energies, and so it was ignored in the analysis.

The cross sections for the $a'^1\Sigma$ and $a^1\Pi$ states of nitrogen are shown in Fig. 7. The $a^1\Pi$ cross section appears to be strongly enhanced at near-threshold energies, and it is significantly larger than that for the $a'^1\Sigma$ state. The magnitude and shape of this cross section is of interest as the main trapping gas which is used in the buffer-gas trap is N_2. Given the operating energies of the various trap stages, it appears that it is this strong enhancement of the $a^1\Pi$ state that is responsible for the efficient trapping of the positrons. The near-threshold behaviour of this cross section indicates the possible presence of a resonance, but this remains to be investigated further. Unfortunately, there are no calculations available to compare with the positron-impact cross section measurements.

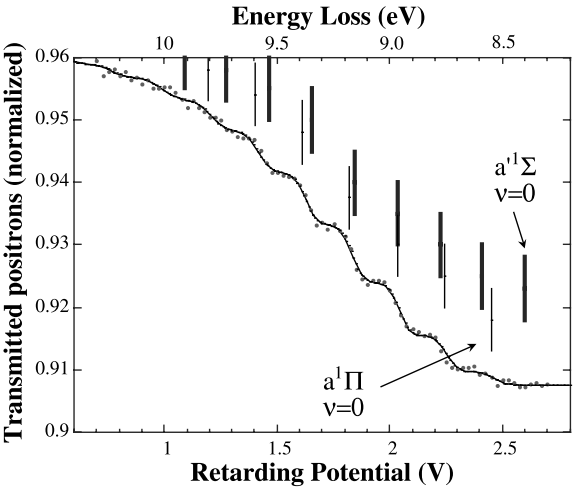

Fig. 6. RPA data for positrons scattered by N_2 at an incident energy of 11 eV. The vertical bars indicate the vibrational levels for the $a'^1\Sigma$ and $a^1\Pi$ states and the solid curve is a fit to the data using known Franck–Condon factors.

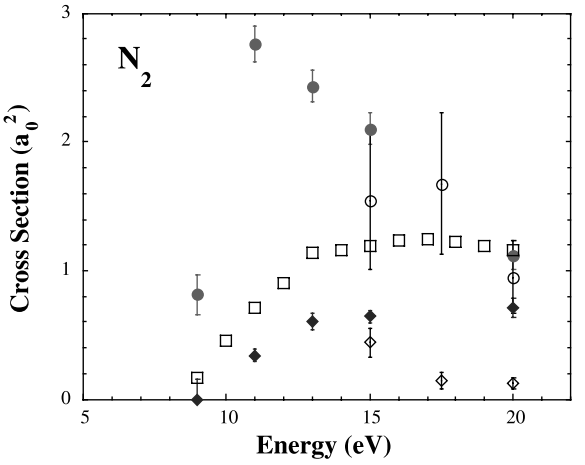

Fig. 7. Absolute integral cross sections for the excitation of the (◆) $a'^1\Sigma$ and (●) $a^1\Pi$ states of N_2 from threshold to 20 eV. The electron scattering data for the (◇) $a'^1\Sigma$ and (○, □) $a^1\Pi$ states are from [34,35].

For H_2, the analysis of the experimental data is more straightforward as the lowest-lying singlet state, the $B^1\Sigma$ state at 11.19 eV, is well isolated from the next excited singlet state at ~11.8 eV. The cross section for this state is shown in Fig. 8. It exhibits a relatively slow rise above threshold to a maximum of ~1.5 a.u. at ~20–25 eV. It can be

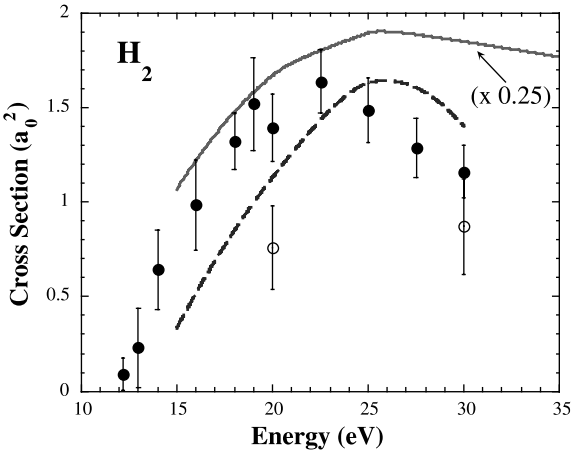

Fig. 8. Absolute integral cross sections for the excitation of the $B^1\Sigma$ state of H_2 from threshold to 30 eV. (•) present data, (—) close coupling [8] and (– – –) Schwinger variational [9] calculations. The close-coupling calculation has been reduced in magnitude by a factor of four. (○) electron scattering data from [44].

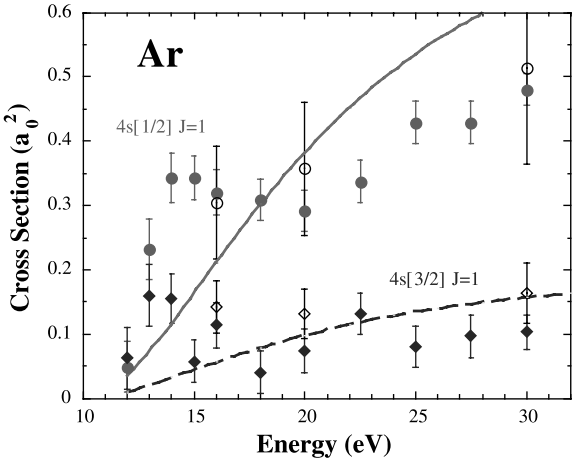

Fig. 9. Absolute integral cross sections for the excitation of the $3p^5$ ($^2P_{3/2,1/2}$) 4s ($J = 1$) states of Ar from threshold to 30 eV. (◆) present data for the $^2P_{3/2}$ state, (– – –) relativistic, distorted-wave theory [30], (•) present data for the $^2P_{1/2}$ state, (—) relativistic, distorted-wave theory [30]. The open symbols are electron scattering data from [45].

compared with two contemporary theoretical calculations, a close-coupling calculation [8] and a Schwinger variational calculation [9]. While both calculations provide a good account of the near-threshold energy dependence of the cross section, the former is about a factor of four larger than the data. Thus, the best description of the cross section is provided by the Schwinger variational calculation.

In argon, the lowest lying (4s) excited-state manifold consists of four states. Two of these, with total angular momenta $J = 0$ and 2, are metastable and are not expected to be excited by positron impact. The remaining two states, the $3p^5$ ($^2P_{3/2,1/2}$) 4s ($J = 1$) levels, are accessible by positron impact, and the cross sections for these excitations are shown in Fig. 9. The cross section for the state coupled to the $^2P_{1/2}$ core level is the largest at near-threshold energies, and structure is evident at energies near 15 eV. These cross sections are compared in the figure with a recent relativistic, distorted-wave calculation [30], which employs multiconfiguration, Dirac–Fock wavefunctions. Such a calculation is not expected to reproduce the structure which is observed at near-threshold energies in the experimental data, but the agreement elsewhere with regard to the absolute magnitude of both excited state cross sections and the overall energy dependence is quite good.

We note that there is no evidence of excitation of triplet states in the experimental data for any of the targets we have studied, all of which possess singlet ground states. Given the absence of the exchange interaction for positron scattering, the only way that such excitations could occur (i.e. which require a spin-flip) would be via the spin–orbit interaction. This interaction is expected to be weak in positron scattering due to the repulsive static potential, and one might expect it to be particularly weak in the targets we have studied due to their relatively low atomic numbers. Nonetheless, this is the first time that such an experimental observation has been possible in any atomic or molecular system for the case of positron impact.

3.4. Feshbach resonances in positron scattering

The possibility of positron resonances has been the subject of considerable interest for many years. Such features, where the projectile binds temporarily to the target atom or molecule, have not

been observed to date in any positron scattering experiment, in contrast to the situation in electron scattering where they *dominate* the scattering for many atomic and molecular systems. There have, however, been several ab initio theoretical estimates which point to the existence of Feshbach resonances in positron scattering by simple atomic targets, such as H and He near the thresholds for the $n = 2$ and 3 excitation of the target and the Ps($n = 2$) threshold. Of particular interest in the present investigation, there has been a recent prediction [31] of a Feshbach resonance associated with the $B^1\Sigma$ state in H_2. This calculation, which uses the Schwinger variational approach, predicts a strong, narrow feature just below the $B^1\Sigma$ state threshold, although its parentage is thought to be a mix of the B- and E-states of H_2.

Experimental confirmation of the existence of resonances has been hampered both by poor energy resolution and low statistical accuracy in measurements using conventional sources and beams. Most positron sources have energy widths which are ~0.5 eV (FWHM) and this renders the observation of narrow resonances quite difficult. One notable exception to this was early work by the Detroit group [32] who conducted a search (unsuccessfully) for resonances in the total scattering cross section for a number of targets using a positron beam with an energy width of ~100 meV.

We have applied a similar approach to search for resonances in the total scattering cross sections for H_2, N_2, CO and Ar at energies near the thresholds for the low-lying excited states of each target. The energy resolution in these measurements is ~25 meV FWHM, and high statistical accuracy was achieved in each case. The data for H_2 are shown in Fig. 10, where we also show in the inset the results of the recent calculation [31]. The calculation shows a resonance in the integral elastic cross section which has a "strength" of $\approx 100\ a_0^2$ meV. We note that the present measurement of the total cross section is not a direct comparison as there are contributions to the TCS from inelastic processes such as vibrational excitation and positronium formation. However, we estimate that these contribute, at most, $\geqslant 25\%$ of the total cross section at energies below the $B^1\Sigma$ state threshold [33], and thus the comparison shown in Fig. 10 is

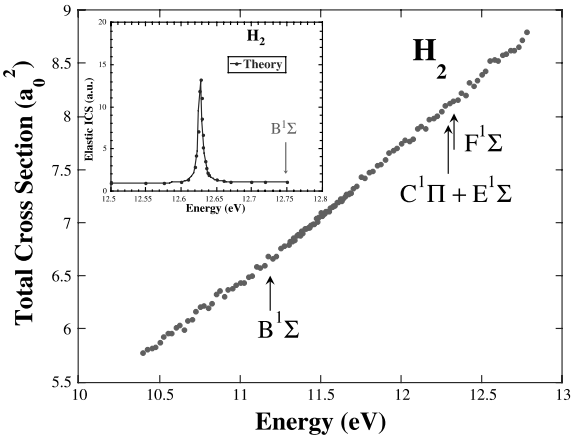

Fig. 10. The total scattering cross section for H_2 in the region of the lowest lying singlet excited states (indicated by arrows on the plot). The inset shows the calculated elastic scattering cross section in this region from [31].

still meaningful. There is clearly no evidence of such a strong resonance feature in the experimental data, and we can place an upper limit of $\sim 2a_0^2$ meV on the strength of any resonance in this region.

Similar measurements in the other gases we have studied (N_2, CO, Ar) also provided negative results, with no evidence of resonance structure in the region of the thresholds of their lowest electronic excited states.

3.5. Comparison with electron scattering cross sections

For some of the excitation cross section measurements presented here, it is possible to make a direct comparison with absolute scattering measurements for electron collisions and some interesting observations follow from these comparisons. With a few exceptions, which we discuss below, the striking aspect of these comparisons is that, in most cases, the cross sections for electron and positron impact are quite similar in magnitude at energies close to threshold. This is surprising given the absence of the exchange interaction for positrons, which is expected to be most significant at low energies, and the different nature of the static potential for electron and positron scattering.

The other striking feature is that the *quality* of the positron scattering data is at least as good as that for the electrons. For the most part, this is due to the fact that the integral cross sections for electron scattering are derived from differential scattering measurements. In most cases, these measurements do not cover the full angular range, and uncertainties involved in extrapolation to forward and backward angles, and subsequent integration, result in large uncertainties in the derived ICS. Given that the present experimental approach can also be readily applied to electron trapping and scattering, there may be some distinct advantages in using these techniques for near-threshold electron impact excitation measurements.

One case where there does appear to be a substantial difference between the electron and positron scattering cross sections is for the near-threshold excitation of the $a^1\Pi$ state of N_2. We see from Fig. 7 that the positron cross section has a sharp rise just above threshold to a maximum which appears to be around 10 eV, in contrast to that for electrons which rises slowly and smoothly to a maximum value at around 15–20 eV [34,35].

4. Energy-resolved measurements of annihilation rates in atoms and molecules

Understanding the process by which a positron annihilates on atoms and molecules is of fundamental importance for a range of areas in science and technology. Examples include, surface characterization [36], positron induced ionization and fragmentation of molecules [37], and atomic and molecular physics [38]. Until now the only available method to study positron annihilation below positronium formation was by measuring annihilation rates of positrons in situ with a molecular target using a thermal (i.e. Maxwellian) distribution of positrons [10–15,39]. Most of these measurements were taken with a thermal positron distribution of 300 K (0.025 eV). One outstanding question first raised by the seminal work of Paul and Saint-Pierre [10] is to understand the enhanced annihilation rates in molecules which are orders of magnitude larger than can be explained on the basis of simple collisions. Using the technique described above to generate a cold positron beam and a new experimental apparatus, we have made the first measurements of positron annihilation on atoms and molecules as a function of beam energy [40]. These results provide direct evidence that the excitation of vibrational resonances in the positron–molecule complex are responsible for the greatly enhanced annihilation rates.

4.1. Description of the experiment

Fig. 11 shows a schematic diagram of the experimental apparatus. The cold positron beam is magnetically guided through an annihilation cell containing the test gas. A constant pressure is maintained in the cell (i.e. typically between 0.02 and 0.1 mTorr) using a controlled feedback system. A capacitance manometer is used to measure the pressure. The beam is operated in a pulsed mode with 2 μs pulses, containing $\sim 5 \times 10^4$ cold positrons at a repetition rate of 4 Hz, with the energy tuned from 50 meV upwards [1]. A CsI detector, light pipe, and photodiode are used to measure the γ-radiation resulting from positron annihilation. The detector is shielded to measure only those γ-rays emitted from a 10 cm region in the annihilation cell.

Due to the small values of the annihilation cross sections, extreme care must be taken to shield against background signals. In addition to γ-ray shielding surrounding the annihilation cell, the detector is gated on only during a 20 μs period coincident with the beam dump. Background noise that would occur from annihilation of the positrons on the collector plate is avoided by keeping the positrons in flight during this time. This is accomplished by placing a potential barrier beyond the annihilation cell, which reflects the positron beam, trapping it between the beam-dump electrode and the reflector plate (see Fig. 11). The resulting background signal is one count per 10^9 positrons dumped, which is well below a typical signal level of one count per 10^7 positrons dumped. The error in the absolute measurements of annihilation rates is estimated to be $\pm 25\%$, based on uncertainties in the gas pressure, the number of positrons per dump, and the detector efficiency.

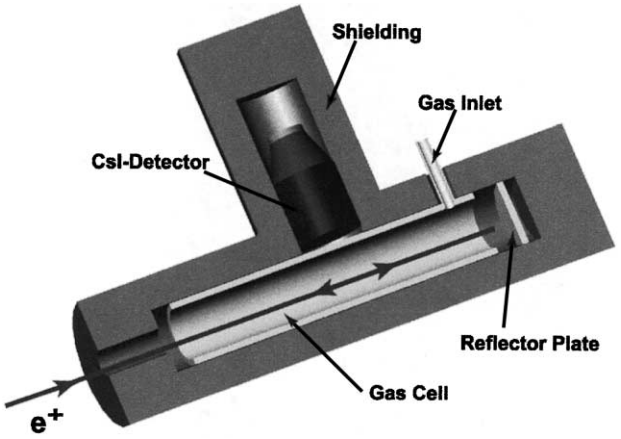

Fig. 11. Schematic diagram of the apparatus used to measure annihilation rates as a function of positron energy. Pulses of monoenergetic positrons pass through the annihilation cell containing a test gas. The γ-rays emitted from the annihilation are detected using a CsI detector.

4.2. Energy-resolved annihilation rate measurements

Fig. 12 shows the annihilation rate for butane (C_4H_{10}) as a function of positron energy. Historically, positron annihilation rates have been measured in terms of the dimensionless parameter Z_{eff}. This rate, Z_{eff}, is scaled by the Dirac annihilation rate for an uncorrelated electron gas at the number density, n_{m}, of the molecular target, thus $Z_{\mathrm{eff}} = \Gamma/\pi r_0^2 c n_{\mathrm{m}}$, where Γ is the annihilation rate, r_0 is the classical radius of the electron, and c is the speed of light. If there were no correlation between the positron and molecular electrons, Z_{eff} would be equal to the number of electrons in the molecule (e.g. which is 26 for butane). The most prominent feature in the data is the large enhancement in Z_{eff} throughout the energy region of the molecular vibrations (see the inset in Fig. 12). A sharp peak is observed at an energy shifted below the C–H stretch mode of 0.36 eV by $\Delta\varepsilon \sim 30$ meV. The value of Z_{eff} at the peak is 23,000, which corresponds to an enhancement of nearly a factor of 900 over that expected from the uncorrelated free-electron model and a factor of two larger than the value measured with a Maxwellian distribution of positrons at 300 K. At energies above those of the vibrational modes, and to within 0.5 eV of the positronium formation threshold (i.e. 3.8 eV), Z_{eff} is $\leqslant 100$.

Other alkanes have also been studied, including propane (C_3H_8) and ethane (C_2H_6), both of which have similar structure to butane with comparably smaller C–H stretch peak values of 10,500 and 900, respectively. In comparison, Fig. 13 shows annihilation rates for ammonia (NH_3) at beam energies from 50 meV to 0.6 eV. There is no prominent peak in the spectrum for this molecule, but there is spectral weight throughout the region

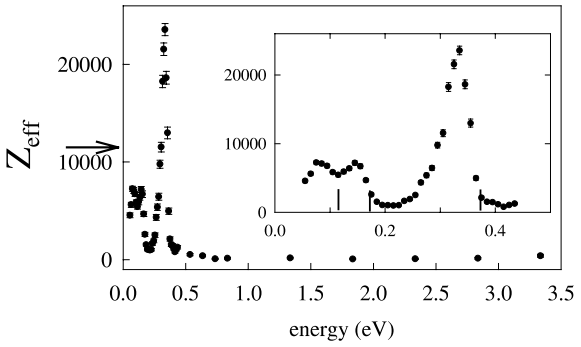

Fig. 12. The first measurement of annihilation rates as a function of positron energy. The annihilation rate, Z_{eff}, for butane (C_4H_{10}) is shown for the energy range from 50 meV to 3.3 eV. The arrow on the vertical axis shows the annihilation rate for a Maxwellian distribution of positrons at 300 K. The inset shows the same data on an expanded scale for positron energies in the range $50 \leqslant \varepsilon \leqslant 420$ meV. Vertical lines on the horizontal axis in the inset indicate the energy of the infrared-active vibrational modes.

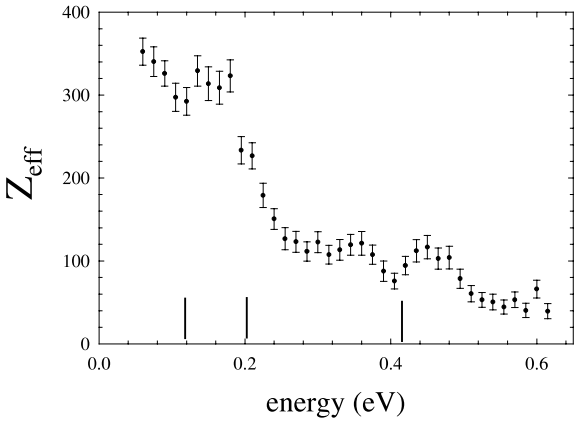

Fig. 13. Normalized positron annihilation rate, Z_{eff}, for ammonia (NH_3) measured in the energy range from 50 meV to 0.6 eV. The vertical lines on the horizontal axis indicate the energies of the vibrational modes.

of vibrational modes. The maximum Z_{eff} measured in ammonia is 350, which is a factor of 4.5 smaller than the value of 1600 measured at 300 K.

While these experiments are still in their infancy, several interesting results have been established. The greatly enhanced values of Z_{eff} that are observed as the positron energy is tuned through the vibrational modes in butane, propane, and ethane show that this enhancement occurs via a vibrational resonance of the positron–molecule complex. A number of theoretical models have attempted to explain the large values of Z_{eff} (300 K) measured in previous experiments [12,15–19,41,42]. The measurements presented here tend to support the model of Gribakin [19], which attributes the large Z_{eff} values to positron capture in vibrational Feshbach resonances [15,19]. In this model, large enhancements of the annihilation rates (e.g. $Z_{eff} > 1000$) are possible only for molecules that have a positron bound state. A positron can then excite a vibrational mode of the positron–molecule complex and become temporarily bound to the molecule, greatly increasing the probability of annihilation. The presence of a bound state is expected to manifest itself by a downward shift in energy of the vibrational resonance equal to the binding energy of the positron–molecule complex. Accordingly, the downward shift of $\Delta\varepsilon = 30$ meV of the butane peak is the most direct evidence to date of such a positron–molecule bound state.

Future improvements in the technique, and extension of the list of molecules studied, can be expected to increase our understanding of the process by which annihilation in molecules occurs. One approach will be to study alkanes larger than butane, such as pentane (C_5H_{12}), hexane (C_6H_{14}), and heptane (C_7H_{16}), which have Z_{eff} (300 K) values much larger than butane. According to Gribakin's model, these molecules are expected to have larger binding energies, and this would, in turn, result in larger downward shifts in the measured C–H vibrational peak from the vibrational mode [15,19]. The mechanism for positron annihilation on small molecules can also be studied. We have evidence that small molecules (e.g. ammonia) have structure throughout the energy region of the vibrational modes. By studying these molecules, where more detailed theoretical calculations and models are possible, we are likely to gain a better understanding of the mechanisms involved in enhancement of the annihilation process. Lastly, investigating annihilation rates just below the threshold for the formation of positronium (and at other inelastic thresholds) should allow us to test the predictions of other models of positron annihilation in atoms and molecules [17,42,46,47].

5. Concluding remarks

We have presented experimental results for a range of positron scattering phenomena which demonstrate the versatility of trap-based positron beams. This technique offers both high energy resolution and high specificity, enabling measurements, for the first time, of absolute cross sections for elastic scattering and state-resolved inelastic scattering processes such as vibrational and electronic excitation. In most cases, this is the first such data to be reported and it provides a basis for comparison with contemporary scattering theories. Where such theory exists the level of agreement is mixed. For example, elastic differential scattering from the most simple molecular target, H_2, shows only a reasonable level of agreement

with theory, while in the case of electronic excitation of Ar, there is good agreement in absolute magnitude with a recent relativistic, distorted-wave calculation. It is hoped that the present data will stimulate further theoretical investigations of low energy positron scattering for a variety of systems, including CO and N_2.

The new scattering technique described here has wide potential application both for positron and electron scattering. We hope to extend the work on near-threshold excitation to a range of other atomic and molecular systems and to also study ionization and positronium formation cross sections. Given the high quality of the present positron cross section measurements as compared with currently available electron scattering data, the extension of the present technique to measurements of near-threshold electron scattering cross sections appears to be justified. Although accurate values for such cross sections are required in a broad range of discharge-based technologies, both the quantity and quality of such data is limited. Given that these cross sections are also often dominated by sharp, negative-ion resonances, they would provide an ideal vehicle for further exploiting the capabilities of the present technique.

We have also discussed briefly a new type of experiment to study positron annihilation, measuring annihilation rates as a function of positron energy with a resolution $\sim$25 meV. The results to date indicate that the greatly enhanced values of Z_{eff} observed in broad classes of molecules are closely associated with the excitation of vibrational resonances of the positron–molecule complexes. The signal-to-noise levels appear to be good enough that small molecules and some atoms can also be studied with precision. There appear to be a number of important future directions for this work, including quantitative tests of models of positron annihilation and understanding the nature of positron–molecule bound states. Another related phenomenon of interest that can now be studied with increased precision is the fragmentation of molecules (including those of biological interest) following positron annihilation, particularly at energies below and/or near the threshold for positronium formation.

Acknowledgements

This work is supported by the National Science Foundation grant 98-76894 and the Office of Naval Research grant N00014-97-1-0366. It is a pleasure to acknowledge the expert technical assistance of Gene Jerzewski. S.J.B. is pleased to acknowledge the support of the Australian-American Fulbright Commission and the University of California, San Diego. We also gratefully acknowledge Bob McEachran and Franco Gianturco for the provision of tabulated data prior to publication and for helpful discussions.

References

[1] S.J. Gilbert et al., Appl. Phys. Lett. 70 (1997) 1944.
[2] L. Dou et al., Phys. Rev. A 46 (1992) 5327.
[3] S. Sur, A.S. Ghosh, J. Phys. B: At. Mol. Phys. 18 (1985) L715.
[4] F.A. Gianturco, T. Mukherjee, P. Paioletti, Phys. Rev. A 56 (1997) 3638.
[5] F.A. Gianturco, T. Mukherjee, J. Phys. B: At. Mol. Opt. Phys. 30 (1997) 3567.
[6] M. Kimura et al., Phys. Rev. Lett. 80 (1998) 3936.
[7] L.A. Parcell, R.P. McEachran, A.D. Stauffer, Nucl. Instr. and Meth. B. 171 (2000) 113.
[8] T. Mukherjee, S. Sur, A. Ghosh, J. Phys. B: At. Mol. Opt. Phys. 24 (1991) 1449.
[9] J.L.S. Lino, J.S.E. Germano, M.A.P. Lima, J. Phys. B: At. Mol. Opt. Phys. 27 (1994) 1881.
[10] D.A.L. Paul, L. Saint-Pierre, Phys. Rev. Lett. 11 (1963) 493.
[11] G.R. Heyland et al., Can. J. Phys. 60 (1982) 503.
[12] C.M. Surko et al., Phys. Rev. Lett. 61 (1988) 1831.
[13] T.J. Murphy, C.M. Surko, Phys. Rev. Lett. 67 (1991) 2954.
[14] K. Iwata et al., Phys. Rev. A 51 (1995) 473.
[15] K. Iwata et al., Phys. Rev. A 61 (2000) 022719.
[16] P.M. Smith, D.A.L. Paul, Can. J. Phys. 48 (1970) 2984.
[17] G. Laricchia, C. Wilkin, Phys. Rev. Lett. 79 (1997) 2241.
[18] E.P. da Silva, J.S.E. Germano, M.A.P. Lima, Phys. Rev. Lett. 77 (1996) 1028.
[19] G.F. Gribakin, Phys. Rev. A 61 (2000) 022720.
[20] S.J. Gilbert et al., Nucl. Instr. and Meth. B. 171 (2000) 81.
[21] E.A.G. Armour, M. Plummer, I. Shimamura, Hyperfine Interactions 89 (1994) 309.
[22] T.L. Gibson, J. Phys. B: At. Mol. Opt. Phys. 25 (1992) 1321.
[23] J.P. Sullivan, S.J. Gilbert, C.M. Surko, Phys. Rev. Lett. 86 (2001) 1494.
[24] D.A. Przybyla et al., Phys. Rev. A 60 (1999) 359.
[25] S.J. Gilbert, R.G. Greaves, C.M. Surko, Phys. Rev. Lett. 82 (1999) 5032.

[26] F.A. Gianturco, T. Mukherjee, Phys. Rev. A 64 (2001) 024703.
[27] P. Baille, J.W. Darewych, Phys. Lett. 35 (1974) 243.
[28] F.A. Gianturco, T. Nishimura, Private Communication, 2001.
[29] J.P. Sullivan et al., Phys. Rev. Lett. 87 (2001) 073201.
[30] R.P. McEachran, A.D. Stauffer, Private Communication, 2001.
[31] M.T.N. Varella, C.R.C. Carvalho, M.A.P. Lima, in: C.M. Surko, F.A.G. Gianturco (Eds.), New Directions in Antimatter Chemistry and Physics, Kluwer, Amsterdam, 2001, p. 493.
[32] T.S. Stein et al., in: International Conference on the Physics of Electronic and Atomic Collisions, Gatlinburg, TN, 1981, p. 424.
[33] C.K. Kwan et al., Nucl. Instr. and Meth. B 143 (1998) 61.
[34] N.J. Mason, W.R. Newell, J. Phys. B: At. Mol. Opt. Phys. 20 (1987) 3913.
[35] L. Campbell et al., J. Phys. B: At. Mol. Opt. Phys. 34 (2001) 1185.
[36] P.J. Schultz, K.G. Lynn, Rev. Mod. Phys. 60 (1988) 701.
[37] L.D. Hulett, Chem. Phys. Lett. 216 (1993) 236.
[38] G.G. Ryzhikh, J. Mitroy, Phys. Rev. Lett. 79 (1997) 4124.
[39] K. Iwata et al., Phys. Rev. A 55 (1997) 3586.
[40] S.J. Gilbert et al., Private Communication, 2001.
[41] V.I. Goldanskii, Y.S. Sayasov, Phys. Lett. 13 (1964) 300.
[42] G. Laricchia, C. Wilkin, Nucl. Instr. and Meth. B 143 (1998) 135.
[43] C.T. Bundschu et al., J. Phys. B: At. Mol. Opt. Phys. 30 (1997) 2239.
[44] M. Khakoo, S. Trajmar, Phys. Rev. A 34 (1986) 146.
[45] A. Chutjian, D.C. Cartwright, Phys. Rev. A 23 (1981) 2178.
[46] J. Mitroy et al., Phys. Rev. Lett. 83 (1999) 3570.
[47] G.G. Ryzhikh et al., J. Phys. B: At. Mol. Opt. Phys. 33 (2000) 2229.